RESEARCH PAPER

PCCP
www.rsc.org/pccp

Experimental and theoretical characterisation of sonochemical cells.

Part 2:† cell disruptors (Ultrasonic horns) and cavity cluster collapse

Peter R. Birkin,*[a] Douglas G. Offin[ab] and Timothy G. Leighton[b]

[a] *School of Chemistry, University of Southampton, Southampton, UK SO17 1BJ*
[b] *Institute of Sound and Vibration Research, University of Southampton, Southampton, UK SO17 1BJ*

Received 2nd November 2004, Accepted 14th December 2004
First published as an Advance Article on the web 12th January 2005

Cavitation theory is used to predict the acoustic pressure at the boundary of the inertial/non inertial threshold for a range of bubble sizes. The sound field generated from a commonly employed sonoelectrochemical cell is modelled. The model is tested with a calibrated hydrophone far from the transducer to avoid spatial averaging. This allows the model to provide the absolute pressure amplitude as a function of axial distance from the source. An electrochemical technique for detecting both inertial and non-inertial cavitation within the solution is employed. This technique uses a dual microelectrode to map the boundary between the regions where inertial cavitation occurs (associated with surface erosion), and where it does not. This zone occurs close to the transducer for the microelectrode employed (<1.5 mm). Further characterisation of the inertial cavitation zone is achieved by imaging of multibubble sonoluminescence (MBSL). The pressures at the boundary between inertial and non inertial cavitation that are determined from the electrochemical and imaging experiments are compared to a sound field model and cavitation theory. Qualitative arguments for the invasive nature of the electrode into the sound field are proposed. Evidence for cavity cluster collapse and shock wave emission is presented and discussed in relation to luminescence, the electrochemical experiments and cavitation theory.

Introduction

The effects of ultrasound on chemical systems have been strongly associated with the phenomena known as cavitation.[1,2] There are many types of cavitation which may form within a liquid under the influence of favourable physical conditions. However, a large proportion of the chemical and physical effects are strongly associated with inertial (transient) cavitation.[2–4] This phenomenon is characterised by the expansion and subsequent rapid collapse of voids or bubbles within a liquid as the result of suitable physical conditions. The generation of inertial cavitation is often achieved through the application of an ultrasonic sound field within a liquid, although some instances of sonochemical effects induced by inertial cavitation can be found employing flows.[5–8] Vibrational and acoustic techniques for the generation of inertial cavitation are attractive because of the apparent ability to control the amplitude and temporal characteristics of the pressure field. However, little attention has been spent in the chemical literature on the spatial characterisation of these acoustic fields. This topic is important because the generation and collapse of cavitation bubbles within a liquid is heavily dependent on the exact physical conditions prevalent at the nucleation point.[3,9] Hence, it is necessary to consider the entire sound field generated from a given source when investigating the possible effects of cavitation and the interpretation of the experimental results.

In this, and a companion paper,[10] the sound field from commonly used electrochemical and sonochemical cell designs are described. Here a combination of electrochemical and acoustic measurements are used to characterise the sound field employed, and predict the threshold for inertial cavitation.

The effects of sonication on electrochemical systems have been widely studied, both in terms of enhanced mass transfer of electroactive species[11–16] and erosion of the electrode surface.[17–19] Here, a novel dual microelectrode is employed to detect both of these effects in a small volume of space within the sonochemical reactor. This can be used to determine the extent and spatial location of inertial cavitation within the cell. The results initially confirm and quantify the widely held view that the sound field generated by ultrasonic cell disruptors of the type used here is in general greatest near the faceplate; and if inertial cavitation is to occur anywhere in the solution, it will occur here first. The threshold for inertial cavitation (in terms of distance from the faceplate) will be determined using imaging[20] and electrochemical techniques; and having located this boundary, the acoustic pressure there is a first-order estimation of the threshold pressure required to generate inertial cavitation. However, two effects complicate measurement of the acoustic pressure amplitude at this location. First, hydrophone signals in continuous-wave cavitation fields are made up of not just the driving field from the transducer, but also bubble-related emissions. Second, and more seriously, the calibrated hydrophone lacks the spatial resolution to measure acoustic pressures here with sufficient accuracy.[3] Workers ignorant of this fact could have unwarranted faith in the output of their hydrophone. In this paper, it is shown how the combined use of an acoustic model and hydrophone measurements can be used to alleviate this problem. Only when account has been taken of all these factors can a realistic test be made of the theory, which predicts the threshold acoustic pressure required to generate inertial cavitation with this ultrasonic horn arrangement.

† For Part 1 see ref. 10.

DOI: 10.1039/b416658b

Theory

Inertial cavitation threshold

The threshold for cavitation has been measured under a number of different physical conditions. Under conditions similar to those reported here, the threshold has been quoted as ~ 1 atm.[21] This is typical of aerated water under standard conditions at low ultrasonic frequencies with, for example, the pressure threshold increasing at higher ultrasonic frequencies. However, it is also possible to calculate the cavitation threshold by employing the approach used by Apfel and Holland.[22] This needs to be done with care, since the calculations of Apfel and Holland were later used by them to derive a 'mechanical index', relevant only to MHz sound fields using pulses having durations of micro-second order[23] (this is now used to give a real-time display during foetal scanning to indicate the likelihood of generating inertial cavitation during that procedure). This theory is adapted here for the very different environment of continuous-wave or tone-burst insonification at frequencies of a few tens of kHz. However, multicycle effects (such as rectified diffusion and population effects[9]) are incorporated only in as much as they are assumed to generate a roughly steady state population with a plentiful supply of nuclei after a few cycles of insonification in gaseous aqueous solution.

As the driving pressure oscillates at any given location in the liquid, the time for which bubble nuclei are subjected to a negative tension whose magnitude exceeds that of the Blake threshold (P_B) is used to calculate the maximum bubble size (R_{max}) attained by the bubble during forced oscillation. Holland and Apfel then use the inferred temperature measurements found in the literature and an adiabatic collapse model to determine whether a particular bubble, under the appropriate physical conditions, can be termed as inertial or non-inertial.[24] Estimates of 'typical' temperatures of a few thousand Kelvin are reported in the literature using a range of assumptions as to what is happening in the interior of the bubble. These estimations date back to 1959 and include the works of Gunther *et al.*[25–28] However, it has also been proposed that if the ratio R_{max}/R_0 exceeds a critical value (~ 2.3) then the cavitation event can also be deemed inertial.[29] These two criteria are termed as either the *temperature* or the *expansive* criteria respectively from this point forward. It is important to recognise that the value for the critical expansion ratio of 2.3 is somewhat artificial. It represents the expansive criterion required to generate bubble wall velocities which exceed linear sound speed in water under equilibrium conditions during the collapse of a cavity. Under these conditions the assumption of incompressibility of the liquid becomes invalid and hence the ratio, $R_{max}/R_0 = 2.3$ reflects the moment at which calculations based on this assumption break down, rather than being based on fundamental physics of inertial cavitation. Nevertheless it is quoted here not only because it has come into common use, but also because Flynn[30,31] showed that at the expansion criterion of around 2, energy concentration in a collapsing bubble is controlled by the inertial forces, a criterion which clearly does reflect the fundamental physics of inertial cavitation. Fig. 1 shows a comparison of these two criteria for determining the pressure threshold for inertial cavitation under standard conditions for an aqueous solution. This figure was constructed by numerically solving the equations described by Holland and Apfel.[22] Bubbles above these thresholds will be classed inertial while bubbles below can be considered non-inertial (stable). Fig. 1 confirms the results of Holland and Apfel, that for very small nuclei (<1 μm) the pressure required to force inertial behaviour increases dramatically with decreasing bubble size, because surface tension forces hinder bubble expansion.[32] It is also apparent that both the *temperature* and the *expansive* criteria under these physical conditions give the optimum radius for cavitation (defined as the bubble size for which the pressure threshold is lowest) to be *ca.* 3 μm. While surface tension effects dominate for smaller bubbles, above this size the pressure threshold gradually rises owing to viscosity and inertial effects associated with the bubble growth.[32] Included on Fig. 1 is the Blake pressure, which demarcates the threshold pressure required for explosive bubble growth but which contains no information on the subsequent collapse. Hence, it can be thought of as representing the minimum criterion for inertial cavitation (*i.e.* necessary but not always sufficient). It is apparent that the *temperature* criterion follows this closely until R_0 reaches *ca.* 3 μm while the expansive criteria deviates over a larger range of R_0. The pressure threshold calculation is informative in showing the range of bubble nuclei with the possibility of inertial cavitation. As the pressure increases then the range of possible nuclei increases. This implies that two phenomena, the increased violence of collapse and the increased number of possible events, are associated with increases of the driving pressure above the threshold required to generate inertial cavitation effects. Higher amplitude driving fields may therefore generate increased effects associated with inertial cavitation (here, increased erosion of the electrode surface). As the following subsection will show, such inertial cavitation zones will tend to occur close to the transducer faceplate (though, as has been shown in a companion paper, it is not true of all transducer geometries).[10]

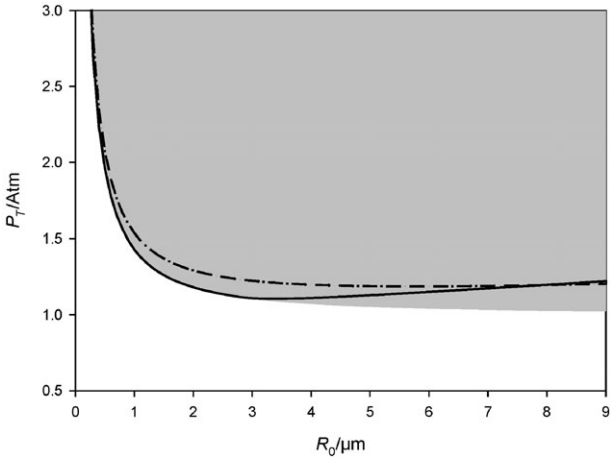

Fig. 1 Plot showing the peak negative threshold pressures, P_T, for inertial cavitation as a function of the initial bubble radii, R_0. The line (---) represents the expansive criterion and (—) represents the temperature criterion. The shaded region shows conditions where bubbles would be expected to be in an environment above the magnitude of the Blake pressure. The plots were calculated using parameters for air bubbles in aqueous solution at 25 °C and an ultrasonic frequency of 22.8 kHz.

Model for field produced by cell disruptor

This paper does not provide an exact model of the field produced by the horn. Instead the models available in standard texts are discussed and applied, in order that the important approximations explained in those texts are highlighted. It should be emphasised that, whilst more sophisticated acoustic models are available; this approach was chosen to make the acoustic element more accessible to the general readership.

Consider the sound field generated by the sources used in ultrasonic cell disruptors and processors of similar design. The simple model used here will treat the emitters as piston-like sources, oscillating linearly, and emitting linear pressure waves into the surrounding media (which is assumed to be homogeneous, isotropic and infinite). The 3D sound field generated from such a sound source can be approximately calculated in the limit by considering the acoustic pressure generated from a piston like emitter, oscillating in simple harmonic mode,[33]

$$P(r,\theta,t) = \mathrm{Re}\left\{ \mathrm{i}\frac{\rho_0 \boldsymbol{c} U_0 k}{2\pi} \int_S \frac{\mathrm{e}^{\mathrm{i}(\omega t - kr')}}{r'} \mathrm{d}S \right\} \qquad (1)$$

where ρ_0 represents the density of the medium, $\boldsymbol{c}$ the velocity of sound within the medium, U_0 the amplitude of the velocity of the piston, k the wavenumber, ω the angular frequency, t the time and r' the distance of the point of interest (where the pressure is being calculated) from an element dS on the surface, S. The Re{} notation indicates that the real component of the expression is taken. This equation allows the prediction of the pressure field within the media. It should be noted that eqn. (1) describes the case where a baffled source (*e.g.* the sound source is in-set into an infinite rigid plane) is employed. If the requirement is to model a non-baffled source,[33,34] for example a disk driven into oscillation in free space, then the energy that propagates into the media in front of the disk is reduced. In this case eqn. (2) would be appropriate.

$$P(r,\theta,t) = \mathrm{Re}\left\{ \mathrm{i}\frac{\rho_0 \boldsymbol{c} U_0 k}{4\pi} \int_S \frac{e^{\mathrm{i}(\omega t - kr')}}{r'} \mathrm{d}S \right\} \qquad (2)$$

However, ultrasonic cell disruptors do not fall directly into either of the groups as they are neither baffled or a freely suspended disk. In fact throughout the tests in this paper (except the electrode mapping shown in Fig. 8, later) the horn was vertical and submerged to a depth of $\sim$15 mm. Since this is much less than the wavelength at 23 kHz (6.4 cm), the closest approximation would be to have the horn baffled by a free surface (although it is noted that the horn will distort the air/water interface). A full simulation of this complex scenario is beyond the scope of this paper. For the purpose of this paper, to a first approximation we can use eqn. (1) to describe the system of interest. The sound field in three dimensions can be calculated numerically using eqn. (1). Analytical solutions can be found for both the axial and 3D case under certain approximations. Kinsler *et al.*[33] gives the following analytical solution for the zero-to-pressure amplitude along the axis of symmetry of the baffled piston, $P_A(r,0)$:

$$P_A(r,0) = 2\rho_0 \boldsymbol{c} U_0 \left| \sin\left\{ \frac{1}{2} kr \left[\sqrt{1 + \left(\frac{a}{r}\right)^2} - 1 \right] \right\} \right| \qquad (3)$$

where a represents the radius of the piston like emitter and r the axial distance away from the sound source.[33] It is convenient at this point to introduce the concepts of near and far fields. Fig. 2 shows the predicted sound field for a 1 cm diameter piston emitting ultrasound at 500 kHz into water compared to the same source operating at 20 kHz. This figure represents the normalised pressure, P_N as a function of r, the distance from the on-axis measurement point to the faceplate of the transducer.

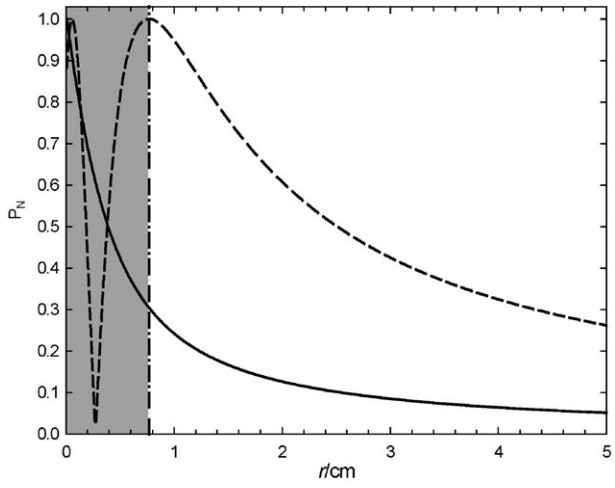

Fig. 2 Plot showing zero-to-peak acoustic pressure amplitude (normalised to the appropriate maximum acoustic pressure amplitude for each curve), P_N as a function of axial distance, r, from the surface of the source for a piston-like emitter (a = 0.5 cm) operating at 500 kHz (--) and 20 kHz (—). The shaded region denotes the near field region for the 500 kHz case. The vertical line (--) indicates the demarcation between the near and far field predicted by eqn. (4) at 500 kHz. The speed of sound was 1480 m s^{-1} and the water density was 1000 kg m^{-3}.

The positions of maxima and minima in pressure will occur with respect to r as predicted by eqn. (4);

$$r_m = \frac{4a^2 - m^2\lambda^2}{4m\lambda} \qquad (4)$$

where m represents an integer value.[33] Maxima are observed for m = 1, 3, 5 *etc*, while minima are observed for m = 0, 2, 4 *etc*. The r_1 value denotes the demarcation from the near to far field (see Fig. 2). However, in most cases, ultrasonic cell disruptors or horns operate under the regime of $\lambda^2 > 4a^2$. Hence, no minima in the variation of the acoustic pressure with distance will be observed. To illustrate this case Fig. 2 shows the sound field generated by a 20 kHz ultrasonic horn with a 1 cm diameter tip

Fig. 2 implies of course that if inertial cavitation is to occur at all with the cell disruptor, it will do so close to the surface of the sound emitter for the 20 kHz case (ignoring the reverberant sound field which under some circumstances can lead to cavitation in other positions[10,35]). As the distance away from the emitter is increased, there will be a point beyond which no inertial cavitation can be detected and only non-inertial cavitation will be observed. Simple geometric divergences of acoustic energy as it propagates away from the source will, of course, predict this. It should, however, be noted that this paper does not incorporate the acoustic effect of the container within which the fluid is replaced. The reverberation caused by such a container can produce fields where the highest amplitudes are produced some distance away from the transducer (as, of course, can result from the use of focused transducers or arrays). This effect is explained in detail in a companion paper.[10] In this current study, this effect becomes most important when measuring the field some distance from the transducer (the 'direct' field dominates the 'reverberant' field close to the faceplate). In order to avoid this complication the hydrophone measurements (used to calibrate the results of the model employed) were performed in a large water tank (measuring 1 m × 2 m × 1 m deep). The use of the tank also allowed the pressure measurements to be made at a distance from the sound source. This avoids spatial averaging due to the finite size of the sensing element within the hydrophone.

The location of the inertial/non-inertial boundary was then determined using electrochemical techniques described in the following section. The pressure at this threshold is estimated using the calibrated model and compared with the predictions of cavitation theory described above.

Attenuation

When sound propagates through a medium away from a source, its amplitude may decrease (attenuate) for a number of reasons. The model described here factors in only one of these mechanisms, specifically geometrical spreading, such that the acoustic power is spread over a larger area thereby decreasing the acoustic intensity at any given point in the liquid. Plane waves of course do not exhibit any geometrical losses. However, they are subject to the other sources of attenuation, such as scattering and absorption (the conversion of acoustic energy ultimately to heat). The following calculation will show that this paper is justified in neglecting these absorption losses associated with bubble free water. The attenuation of plane waves in water can be calculated[36] from eqn. (5).

$$\left(\frac{I_d}{I_0}\right) = \mathrm{e}^{-2\alpha d} \qquad (5)$$

where I_0 is the initial intensity, I_d the intensity after distance d and α the attenuation coefficient. For bubble free water[36] at 25 °C the plane wave absorption coefficient, α, is 1.16×10^{-7} neper cm^{-1} at 23 kHz. Hence, the reduction in the intensity of plane waves over a 10 cm distance is $<3 \times 10^{-4}$%. This indicates that the pressure variations recorded in the large water tank as a function of distance in the absence of cavitation are due to geometric losses and not as the result of absorption of sound by the liquid. The presence of bubbles within a liquid has the effect of increasing the attenuation coefficient.[37] However, without accurate knowledge of the bubble population, this effect is hard to quantify analytically. Nevertheless, the presence of bubbles will undoubtedly cause attenuation. This implies that the threshold pressures quoted here are underestimates.

Experimental

Generation of ultrasound

Ultrasound and cavitation were generated by means of a Grundig Digimess FG 100 function generator, Brüel & Kjær Type 2713 power amplifier and ultrasonic transducer fitted with a 3 mm diameter titanium tip (Adaptive Biosystems). The function generator was interfaced with a PC using software written in-house, allowing the frequency, input voltage and duration of the ultrasound to be accurately controlled. The driving frequency employed was 22.85 kHz.

Electrochemical experiments

All electrochemical experiments were performed using the experimental set-up reported previously[11] although with the addition of an XY stage. The dual electrode[38] consisted of lead (125 μm diameter, 99.5%, Goodfellow) and insulated platinum (50 μm diameter, 99.99%, Goodfellow) microdiscs housed in close proximity in epoxy resin (Struers, Epofix). After manufacture, the electrodes were polished with silicon carbide paper followed by aqueous alumina slurries (1.0 μm and 0.3 μm). Current time histories were measured by means of a home built potentiostat interfaced with a PC through an ADC card (Measurement Computing PCI-DAS 4020/12) and software written in-house. The reference electrode was SCE and a platinum mesh served as the counter electrode. The cylindrical glass cell (internal diameter 67 mm, height 105 mm) was placed on the XY stage, which allowed 25 mm of movement in each direction with 10 μm resolution. This enabled the position of the electrode, placed in the bottom of the cell, to be accurately controlled. The separation between the ultrasonic horn and the electrode was controlled by means of a micrometer and stage, which allowed the vertical position of the transducer (and hence the horn) to be adjusted with 10 μm resolution over a range of 25 mm. In all experiments the cell was filled with 70 cm^3 of solution (20 mM $K_4Fe(CN)_6$ and 0.75 M Na_2SO_4) and the working electrode positioned such that the tip was ~15 mm below the surface of the liquid. For all experiments the temperature of the cell was maintained at 25 °C by means of a water jacket and thermostatic bath. A Faraday cage was used to reduce electrical noise.

Acoustic pressure measurements

Acoustic pressure measurements were made using a Brüel & Kjær 8103 hydrophone and 2635 charge amplifier. For the measurements in water a large tank (measuring 1 m × 2 m × 1 m) was used, and for castor oil a 5 dm^3 beaker (diameter 20 cm) was employed. The large size of the container was necessary to ensure that pressure measurements were made in the direct sound field of the ultrasonic source (as opposed to the reverberant field[10]). The tip of the disruptor was placed 15 mm below the surface of the water, and the hydrophone was positioned such that its acoustic centre was on the axis of symmetry of the disruptor. For the experiment in water the hydrophone was moved on the axis of symmetry by means of a computerised scanning rig. The output of the charge amplifier was recorded by means of an oscilloscope and PC. All pressure measurements are quoted with reference to the centre of the acoustic element within the hydrophone (using data supplied by the manufacturer).

Chemicals and solutions

All solutions were made up using water from an USF Elga Purelab Option E10 water purification system. Water purified in this manner had a conductivity of below 0.1 μS cm^{-1} and a low organic content (TOC < 30 ppb). Na_2SO_4 (BDH, AnalaR), $K_4Fe(CN)_6$ (Aldrich, 99%) and castor oil (Aldrich) were used as received.

Photographic experiments

A Starlite Xpress HX5BC cooled 16 bit CCD camera was used to image luminescence produced by the cavitation induced by the ultrasonic horn. The exact experimental conditions are given in the appropriate figure legends.

Results

Validation of eqn. (3)

In order to validate eqn. (3), the acoustic pressure amplitude, P_A, was measured as a function of axial distance from the sound source. The drive voltage applied to the transducer was low, such that the pressure signal was sinusoidal (see Fig. 3 insert; this was confirmed by FFT analysis of the waveform (not shown)) and there were no audible or visual signs of acoustic cavitation. Fig. 3 shows that a good fit (black line) between the experimental data and eqn. (3) was obtained.

Pressure distance dependence in the presence of cavitation

Having shown that the sound field model was valid in the absence of cavitation a similar experiment was performed in the presence of cavitation. In this case the pressure was again measured on axis using the hydrophone in a large water tank. However, in this experiment cavitation (as indicated by the auditory and visual observations of the system) was produced by increasing the voltage amplitude applied to the transducer. Fig. 4 shows an example of the pressure signal recorded with a hydrophone under these conditions. Clearly, this is a more complex pressure signal than the signal recorded in the absence

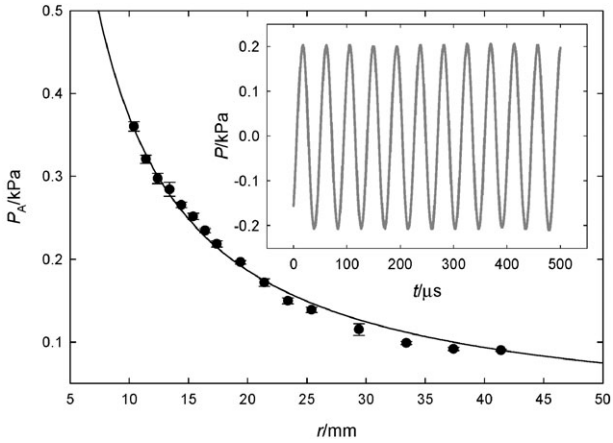

Fig. 3 Plot showing the measured axial pressure amplitude (P_A) as a function of distance, r, (●) and the fit to eqn. (3) (—) in the absence of inertial cavitation. The insert shows a sample of the pressure (P) signal recorded with a hydrophone (—).

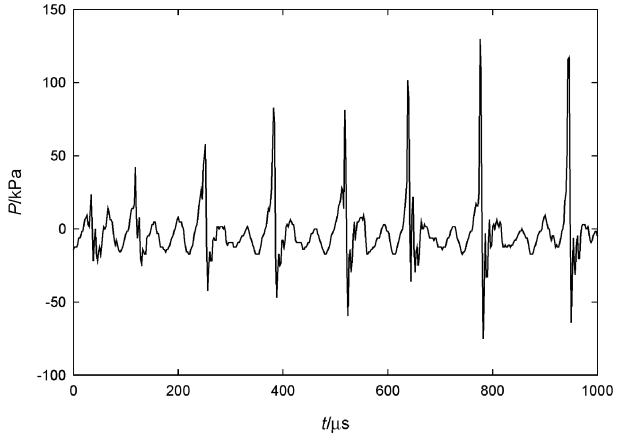

Fig. 4 Plot showing the pressure (P) as a function of time recorded using a calibrated hydrophone in a water tank above the cavitation threshold. The distance between the tip of the ultrasonic source and the acoustic centre of the hydrophone was 8.8 mm.

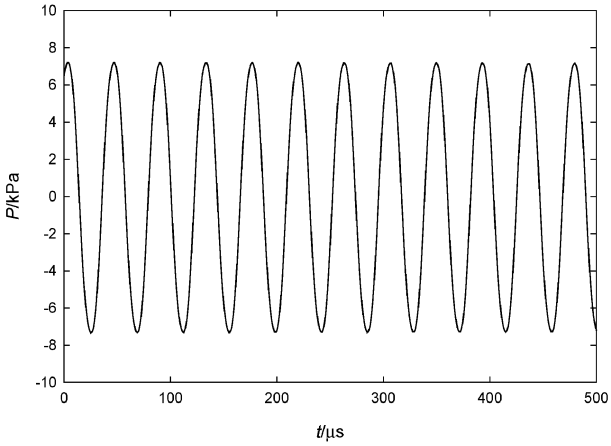

Fig. 5 Plot showing the pressure (P) time signal recorded in castor oil in a 5 dm^3 beaker. The distance between the active element of the hydrophone and the source was 9.55 mm. All other conditions are reported in Fig. 4.

of cavitation (insert to Fig. 3). There is an underlying pressure wave (at the drive frequency of 22.8 kHz), superimposed with spikes (shocks) in the signal, which occur on every third cycle. Pressure shocks produced by cavitation have been associated with cavity cluster collapse. Vyas and Preece suggested that erosion of materials in such cavitation environments was dominated by shocks emitted by a bubble cloud and not the effect of individual bubble jetting.[39] Subsequently Hansson *et al.* produced models and further experimental verification of the dynamics of cavity clusters.[40,41] In short Hansson *et al.* propose that a cluster of bubbles collapse in a hemispherical pattern transferring the energy of each bubble collapse to a final bubble event that causes damage at the solid/liquid interface. If it is assumed that the pressure shocks reported in Fig. 4 were caused by emissions from collapsing bubble clouds, then the amplitude of the both the underlying wave (which generates the initial collapse that triggers the other bubbles in the cluster to collapse) and these pressure shocks (which will travel through the liquid away from the horn (see later argument) is important when determining the threshold pressure for inertial cavitation in the system. However, this assumption must be made with caution and will be tested in this paper. It is possible that the spikes are an intrinsic property of the transducer when driven at the high voltages used to generate cavitation, and rather than being the result of cavitation the spikes are the cause of the phenomenon (the manufacturers were unable to advise on the origin of the $\omega/3$ signal). In order to confirm which of the above scenarios was true, the pressure signal was measured using the same conditions as Fig. 4, but in 5 dm^3 castor oil rather than water. Fig. 5 shows that, as well as there being no audible or visual signs of cavitation in the castor oil sample, the recorded pressure wave was sinusoidal at the selected drive frequency. This indicates that the spikes seen at high drive voltages in water are not due to the properties of the transducer, but the result of emissions from cavitation. As the initial collapse of the cavity cluster will be associated with the driving signal from the ultrasonic horn, it is necessary to isolate the underlying pressure wave from components originating from bubble processes. This was achieved by FFT analysis of the hydrophone signals. Fig. 6 shows the magnitude of the FFT component at the driving frequency plotted as a function of the distance between the centre of the active element within the hydrophone and the tip of the ultrasonic source. The solid line in the figure shows the fit of the experimental data to eqn. (3). This represents the axial pressure field generated by the sound source in the absence of any electrode. Again a good fit between the pressure signal and the theoretical description of the sound field was obtained.

Position of inertial cavitation threshold-MBSL

To locate the spatial boundary between regions where inertial cavitation and non-inertial cavitation exists, a series of experiments were performed. In these experiments it is assumed that the inertial threshold matches the threshold for MBSL. This assumption, associated with the transient threshold, has been made by other investigators.[42] In the first an image of the luminescence produced through MBSL was recorded for the ultrasonic horn operating in the absence of an electrode. Fig. 7 shows an image of the tip of the ultrasonic horn recorded under normal light conditions and in a dark room (images 'a' and 'b' respectively). The boundary between regions of inertial and non-inertial cavitation is assumed to be indicated by the boundary between luminescence and regions of the liquid were no luminescence can be observed. Fig. 6 shows that this boundary extends to a maximum distance of 0.9 $\pm$ 0.05 mm and occurs on the axis as expected from the sound field (see above). It is possible to use the MBSL data and the sound field measurements and fit from the model to predict the threshold pressure for inertial cavitation. Fig. 6 shows that at 0.9 mm the acoustic pressure was 85 $\pm$ 3 kPa. This is clearly lower than the inertial cavitation threshold predicted at 112 kPa. However,

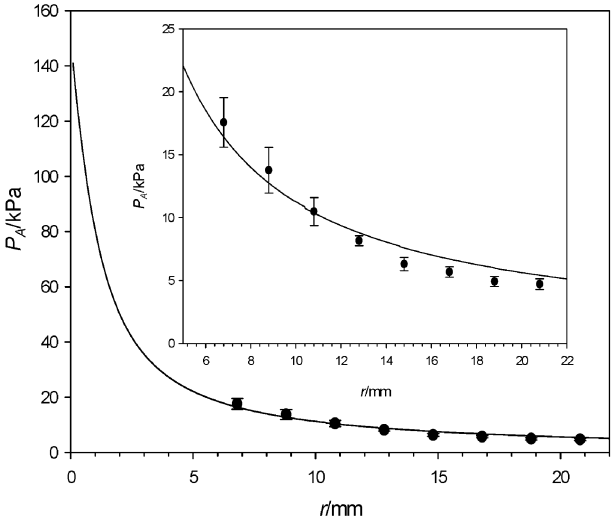

Fig. 6 Plot showing P_A the measured axial pressure amplitude (●) as a function of the separation between the active element of the hydrophone and the tip of the ultrasonic source (r). The solid line (—) represents the fit of the data to eqn. (3). The insert shows an enlargement of the data between 5 and 25 mm.

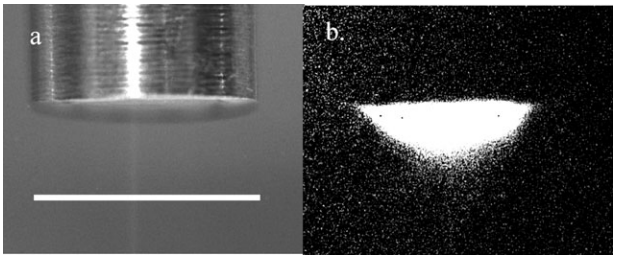

Fig. 7 Images of ultrasonic horn and electrode taken with a cooled CCD camera. Frames (a) was taken under normal daylight conditions while (b) was taken in a dark room. Frame (a) shows the ultrasonic horn its own and (b) the corresponding light emission (exposure time 10 min) in the presence of continuous ultrasonic irradiation (22.85 kHz, 56 W cm^{-2}). The solution contained 0.75 mol dm^{-3} Na_2SO_4. The experiment was performed under ambient conditions (25 °C, aerobic solutions). The scale bar (relevant for image (a) and (b)) represents 3 mm.

the threshold calculation does not take into account the shock waves emitted through cavity cluster collapse. It should be noted that the shock waves occur at the pressure maximum in the driving signal (see Fig. 4). Hence bubbles which are initially compressed by the driving pressure signal at 22.8 kHz are also exposed at this point to a high pressure shock. As the pressure maximum from the shock exceeds‡ 130 kPa at 8.8 mm compared to 14 kPa from the driving signal (22.8 kHz), one can expect the shock pressures to scale up in excess of 10 bar close to the tip of the ultrasonic probe. Clearly these high pressure shocks can collapse bubbles which are sub-inertial, giving rise to luminescence at a greater distance than expected. This supports the diagnosis of the underestimation of the inertial threshold produced if the presence of these spikes is neglected.

Position of inertial cavitation threshold-electrochemistry

A second measure of the spatial extent of the inertial threshold was undertaken. In these experiments a novel electrochemical erosion technique was employed. A dual microelectrode constructed out of a Pb and Pt microdiscs were used to locate the centre of the plume and then probe the erosion boundary which is linked to the inertial cavitation threshold. The construction and deployment of this electrode is described in detail elsewhere.[38]

In this experiment a solution containing sulphate ions and a redox active species ($Fe(CN)_6^{4-}$) was employed. The potential of the microdiscs was held at +0.8 V *vs.* SCE, which results in mass-transfer-limited oxidation of $Fe(CN)_6^{4-}$ at the platinum electrode and passivation of the lead electrode with an insoluble layer of $PbSO_4$. Under these conditions the platinum electrode is sensitive to any process, which results in fluid motion and deformation of the diffusion layer, such as acoustic streaming, bubble motion and both inertial and non-inertial cavitation. These are detected as increased anodic current due to enhanced mass transfer.[16,43] In contrast the lead electrode is only sensitive to inertial cavitation events of sufficient energy to erode the electrode surface. These events can be detected as repassivation transients.[17]

The experimental protocol was as follows. First, the centre of the plume generated by the ultrasonic horn was found by mapping the enhancement in mass transfer of $Fe(CN)_6^{4-}$ to the platinum electrode in a plane below the tip. This was done at a distance (6 mm tip to plane of electrode motion) where no erosion was detected, in order to protect the soft lead sulphate modified electrode from damage. Fig. 8 shows a schematic of

‡ It should be noted that the 8103 hydrophone has an upper frequency limit of ~180 kHz after which the signal begins to be attenuated. Hence these estimations of shock pressure are likely to be underestimations of the real signal.

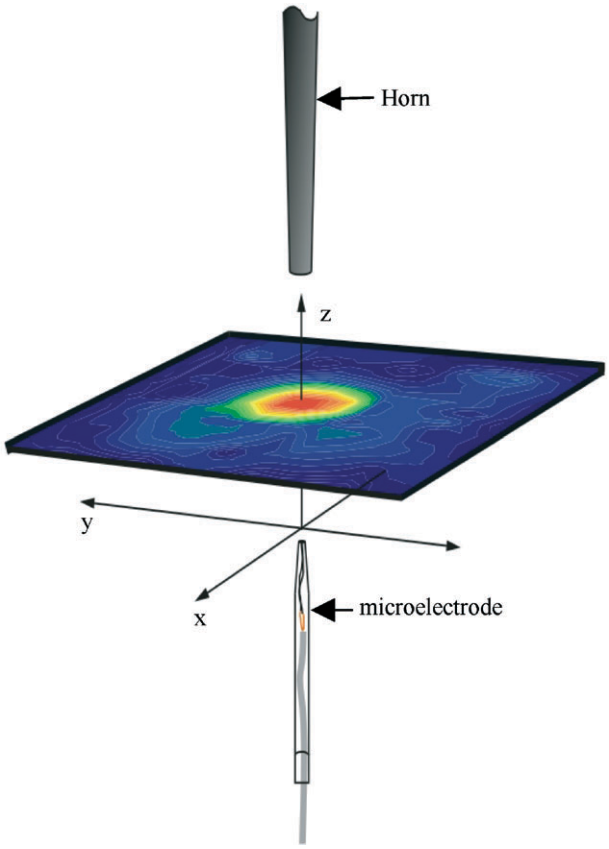

Fig. 8 Schematic showing the experimental protocol for centering the dual electrode and approaching the ultrasonic tip. See Fig. 9 for an indication of the length scales involved.

the experimental approach adopted and Fig. 9 shows a map of the mass transfer enhancement recorded. Second, the microelectrode was placed in the centre of the mass transfer maximum and the current at the lead sulphate modified electrode recorded for a fixed time (0.4 s) at decreasing electrode to tip separations. Fig. 10 shows the number of erosion current

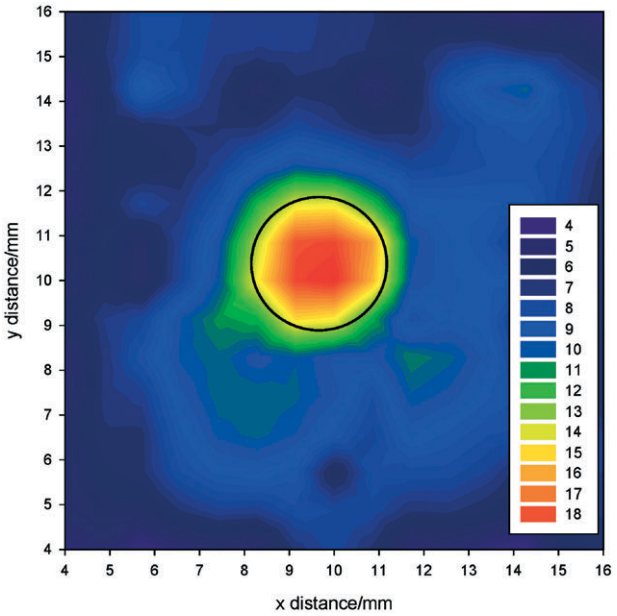

Fig. 9 Contour map showing mass transfer signal at a constant *z* distance (6 mm tip to plane of electrode motion). The electrode was held at +0.8 V *vs.* SCE. The circle indicates the size of the tip of the ultrasonic horn employed. The scale bar indicates the average current normalised to the silent steady state current (132 nA).

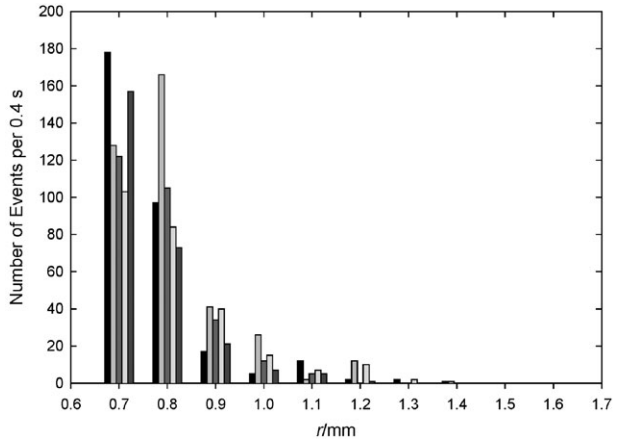

Fig. 10 Plot showing the number of erosion events per 0.4 s determined as a function of z displacement (denoted as r) in the centre of the cavitation plume. The figure shows the results from five repeat experiments.

transients detected. These were counted at each distance using a peak finding program. The boundary between the inertial cavitation region in the liquid (where erosion is expected) and the non-inertial region (where no erosion is expected) was measured under these conditions at 1.3 ± 0.2 mm. This is clearly significantly further than the boundary measured by MBSL and corresponds to an acoustic pressure (as predicted by eqn. (3)) at the boundary between inertial and non-inertial bubble events of 68.8 ± 6.5 kPa. This disagreement could be the result of a number of factors. First, as shown previously, the pressure measurements clearly show a shock emission from the cavitation process. These shocks are not accounted for in the predictions gained from eqn. (3). Shock waves are known to cause damage to solid surfaces. Hence the erosion of the solid/liquid interface of the dual microelectrode will pick up these events if sufficiently energetic. Second, the electrode cannot be regarded as non-invasive as it will, depending on the frequency of the pressure fluctuation considered, the materials employed and the geometry, affect the results observed. These effects are discussed in detail in a companion paper.[44] However, it is predicted that the shocks emitted by the cavity collapse will be reflected by the dual microelectrode tip. This will cause further collapse of cavitation bubbles in front of the dual microelectrode, extending the spatial extent of inertial cavitation.

Consequences

The consequences for the measurement of electrochemical effects of acoustic cavitation are extensive. Clearly the position of the electrode within the sound field will determine the type of cavitation event detected. This will include both inertial and non-inertial events. The exact behaviour will be dependent on the local pressure, the materials employed in the experiment and the bubble population within the local environment.[44] These considerations have not been well documented previously in the sonochemical literature, and may help to explain the differences in the observed type of events reported by different groups. As well as mass transfer effects, the chemical effects of cavitation are also likely to be highly spatially dependent. Inertial cavitation can only be expected close to the tip of the ultrasonic horn. The vast majority of the solution will be exposed to non-inertial or stable cavitation. Clearly the interpretation of the effects of power ultrasound must consider the geometry of the system employed, the materials involved and the bubble population before sensible global conclusions can be drawn. Lastly in order to obtain meaningful results, it is clearly necessary to control the distance between the ultrasonic tip and the electrode substrate with a high degree of accuracy (*e.g.* an accuracy of at least ± 100 μm is desirable) as well as understanding the physical acoustics of the experimental set-up.

Conclusions

The threshold for inertial cavitation (at 23 kHz under standard conditions in water) was estimated using both a luminescence technique and an electrochemical erosion sensor. Inertial cavitation thresholds were predicted for this system. This was achieved by a first order prediction of the sound field produced by a horn placed in a rigid baffle. The limitations of this model are recognised. Combining this model with the experimental measurements of the inertial/non-inertial boundary (from MBSL or electrochemical erosion) gave an underestimation of the pressure threshold. This underestimation is attributed to the pressure spikes generated by the cavitation process. Hence the model (see eqn. (3)) is only valid to a first approximation and requires refinement to consider the pressure spikes and free surface boundary conditions present in the experimental set-up.

Acknowledgements

We thank the EPSRC for funding a studentship for DGO under research grant GR/N30989/01.

References

1 G. J. Price, *Introduction to Sonochemistry*, Royal Society of Chemistry, Cambridge, 1992.
2 T. J. Mason, *Sonochemistry: The Uses of Ultrasound in Chemistry*, Royal Society of Chemistry, Cambridge, 1990.
3 T. G. Leighton, *The Acoustic Bubble*, Academic Press, London, 1994, sections 1.2.2, 4.3.1 and 4.3.2.
4 O. Dahlem, J. Reisse and V. Halloin, *Chem. Eng. Sci.*, 1999, **54**, 2829.
5 K. S. Suslick, M. M. Ndleleni and J. T. Ries, *J. Am. Chem. Soc.*, 1997, **119**, 9303.
6 Y. Yan and R. B. Thorpe, *Int. J. Multiphase Flow*, 1990, **16**, 1023.
7 N. P. Vichare, P. R. Gogate and A. B. Pandit, *Chem. Eng. Technol.*, 2000, **23**, 683.
8 T. G. Leighton, M. Farhat, J. E. Field and F. Avellan, *J. Fluid Mech.*, 2003, **480**, 43.
9 T. G. Leighton, *Ultrason. Sonochem.*, 1995, **2**, S123.
10 P. R. Birkin, T. G. Leighton, J. F. Power, M. D. Simpson, A. M. L. Vinçotte and P. F. Joseph, *J. Phys. Chem. A*, 2003, **107**, 306.
11 P. R. Birkin and S. Silva-Martinez, *J. Electroanal. Chem.*, 1996, **416**, 127.
12 C. R. S. Hagan and L. A. Coury, *Anal. Chem.*, 1994, **66**, 399.
13 J. Klima, C. Berard and C. Degrand, *J. Electroanal. Chem.*, 1995, **399**, 147.
14 J. P. Lorimer, B. Pollet, S. S. Phull, T. J. Mason, D. J. Walton and U. Geissler, *Electrochim. Acta*, 1996, **41**, 2737.
15 F. J. Del-Campo, J. Melville, J. L. Hardcastle and R. G. Compton, *J. Phys. Chem. A*, 2001, **105**, 666.
16 P. R. Birkin and S. Silva-Martinez, *J. Chem. Soc., Chem. Commun.*, 1995, 1807.
17 P. R. Birkin, R. O'Connor, C. Rapple and S. Silva-Martinez, *J. Chem. Soc., Faraday Trans.*, 1998, **94**, 3365.
18 G. O. H. Whillock and B. F. Harvey, *Ultrason. Sonochem.*, 1997, **4**, 23.
19 S. A. Perusich and R. C. Alkire, *J. Electrochem. Soc.*, 1991, **138**, 700.
20 H. N. McMurray and B. P. Wilson, *J. Phys. Chem. A*, 1999, **103**, 3955.
21 W. J. Galloway, *J. Acoust. Soc. Am.*, 1954, **26**, 849.
22 C. K. Holland and R. E. Apfel, *IEEE Trans. Ultrason. Ferroelectr. Freq. Control*, 1989, **36**, 204.
23 R. E. Apfel and C. K. Holland, *Ultrasound Med. Biol.*, 1991, **17**, 179.
24 R. E. Apfel, in *Methods in Experimental Physics*, ed. P. D. Edmonds, Academic Press, New York, 1981, **vol. 19**.
25 K. S. Suslick, D. A. Hammerton and R. E. Cline, *J. Am. Chem. Soc.*, 1986, **108**, 5641.

26 P. Gunther, E. Heim and H. U. Borgstedt, *Z. Electrochem.*, 1959, **63**, 43.
27 P. Gunther, E. Heim and G. Eichkorn, *Z. Angew. Phys.*, 1959, **11**, 274.
28 E. B. Flint and K. S. Suslick, *J. Am. Chem. Soc.*, 1989, **111**, 6987.
29 R. E. Apfel, *Cavitation and Inhomogeneities in underwater acoustics*, Gottingen, July 9–11, 19791980W. Lauterborn, Springer-Verlag, 79.
30 H. G. Flynn, *J. Acoust. Soc. Am.*, 1975, **57**, 1379.
31 H. G. Flynn, *J. Acoust. Soc. Am.*, 1975, **58**, 1160.
32 T. G. Leighton, *The Acoustic Bubble*, Academic Press, London, 1994, section 4.3.1.
33 L. E. Kinsler, A. R. Frey, A. B. Coppens and J. V. Sanders, *Fundamentals of Acoustics*, John Wiley & Sons, New York, 1982.
34 P. M. Morse, *Theoretical Acoustics*, McGraw Hill, New York, 1968.
35 L. A. Crum and G. T. Reynolds, *J. Acoust. Soc. Am.*, 1985, **78**, 137.
36 G. W. C. Kaye and T. H. Laby, *Tables of Physical and Chemical Constants and some Mathematical Functions*, Longmans, Green and Co., London, 1959.
37 T. G. Leighton, *The Acoustic Bubble*, Academic Press, London, 1994.
38 P. R. Birkin, D. G. Offin and T. G. Leighton, *Electrochem. Commun.*, 2004, **6**, 1174.
39 B. Vyas and C. M. Preece, *J. Appl. Phys.*, 1976, **47**, 5133.
40 I. Hansson and K. A. Morch, *J. Appl. Phys.*, 1980, **51**, 4651.
41 I. Hansson, V. Kedrinskii and K. A. Morch, *J. Phys. D: Appl. Phys.*, 1982, **15**, 1725.
42 R. A. Roy, A. A. Atchley, L. A. Crum, J. B. Fowlkes and J. J. Reidy, *J. Acoust. Soc. Am.*, 1985, **78**, 1799.
43 J. Klima, C. Bernard and C. Degrand, *J. Electroanal. Chem.*, 1994, **367**, 297.
44 P. R. Birkin, D. G. Offin, P. F. Joseph and T. G. Leighton, 2005, in preparation.